Phase Transformation Behavior of Gamma Titanium Aluminide Alloys during Supertransus Heat Treatment

S.L. SEMIATIN, V. SEETHARAMAN, D.M. DIMIDUK, and K.H.G. ASHBEE

Microstructure evolution in a wrought near-gamma titanium alloy, Ti-45Al-2Cr-2Nb, was investigated by a series of heat treatments comprised of initial heating high in the alpha-plus-gamma phase field followed by short-time heating in the single-phase alpha field. The initial heating step led to a dispersion of gamma particles which pinned the alpha grain boundaries. The kinetics of the gamma grain dissolution during subsequent heating in the single-phase field were interpreted in terms of models for both interface reaction–controlled and diffusion-controlled processes. The model for diffusion-controlled dissolution yielded predictions comparable to the observed times, whereas the model for interface reaction–controlled behavior predicted dissolution kinetics over an order of magnitude slower than observed. The growth of the alpha grains, both before and after the dissolution of the gamma phase, was also modeled. Section size limitations to the ability to use supertransus heating to obtain uniform and moderately fine alpha grain sizes were examined using the transformation models and a simple heat transfer analysis approach. The results were validated through the heat treatment of subscale and full-scale forgings.

I. INTRODUCTION

THE emergence of a new class of aerospace alloys based on the ordered, face-centered tetragonal, or gamma, phase of the titanium-aluminum system has brought the promise of exceptional improvements in the performance of jet engines.[1] Intended for service at high temperatures approaching or equaling those for which superalloys have typically been used, these so-called gamma titanium aluminide alloys pose significant challenges during processing to useful shapes. Among the most serious obstacles to overcome have been those associated with the wrought processing of ingot metallurgy product forms. Such difficulties are not unexpected in view of the restricted temperature range for deformation processing and the limited hot workability which these alloys exhibit. Nevertheless, a fair amount of success has been achieved in both primary processing of these materials *via* extrusion or forging as well as during secondary processing such as by sheet rolling, closed-die forging, or superplastic sheet forming.[2–8]

Much of the recent research and development on the thermomechanical processing of the gamma titanium aluminide alloys has dealt with materials containing a small amount of the alpha-two (or beta) phase in addition to the gamma phase. The incorporation of the second phase in these near-gamma alloys, coupled with working in the two-phase (alpha plus gamma) field, has led to substantial improvements in hot workability and the ability to obtain very fine microstructures of equiaxed gamma analogous to the equiaxed alpha structures found in many conventional titanium alloy mill products. The equiaxed gamma materials provide good ductility and strength, but inferior fracture toughness and creep resistance. For this reason, considerable effort is now being expended to develop approaches for obtaining alternate microstructures with a better balance of properties.

Near-gamma alloys containing a fully lamellar microstructure with a moderately small ($\approx$50 to 200 μm) alpha grain size have been found to provide the desired better property mix.[9] Several processing techniques have been developed to obtain such microstructures. These methods include extrusion at temperatures within a narrow window around the alpha transus (temperature at which alpha + gamma $\rightarrow$ alpha), or the supertransus heat treatment of alloys containing grain growth–inhibiting elements, such as boron, in solid solution or in the form of precipitates.[10,11,12]

The work described in this article dealt with the general problem of using the supertransus heat treatment of near-gamma titanium aluminide alloys to obtain fully lamellar microstructures. In particular, the control of the alpha grain size in alloys *not* containing grain growth–inhibiting elements was addressed. The specific objective of the work was to develop models of gamma phase dissolution and alpha grain growth during supertransus heating. To this end, samples of a typical near-gamma titanium aluminide were supertransus heat treated using various temperatures and times to establish particle dissolution and grain growth behaviors. The data were interpreted in terms of a suite of phase transformation models as well as a simple heat transfer analysis utilized to quantify temperature-transient effects.

S.L. SEMIATIN, Senior Scientist, Materials Processing/Processing Science, D.M. DIMIDUK, Research Leader, Structural Materials Group, Metals, Ceramics, and NDE Division, and K.H.G. ASHBEE, Visiting Scientist, Processing Science Group, Metals, Ceramics, and NDE Division, are with the Materials and Manufacturing Directorate, Air Force Research Laboratory, WL/MLLM, Wright-Patterson Air Force Base, OH 45433. V. SEETHARAMAN, Senior Scientist, is with the Materials and Processes Division, UES, Inc., Dayton, OH 45432.

This article is based on a presentation made in the symposium ''Fundamentals of Gamma Titanium Aluminides,'' presented at the TMS Annual Meeting, February 10–12, 1997, Orlando, Florida, under the auspices of the ASM/MSD Flow & Fracture and Phase Transformations Committees.

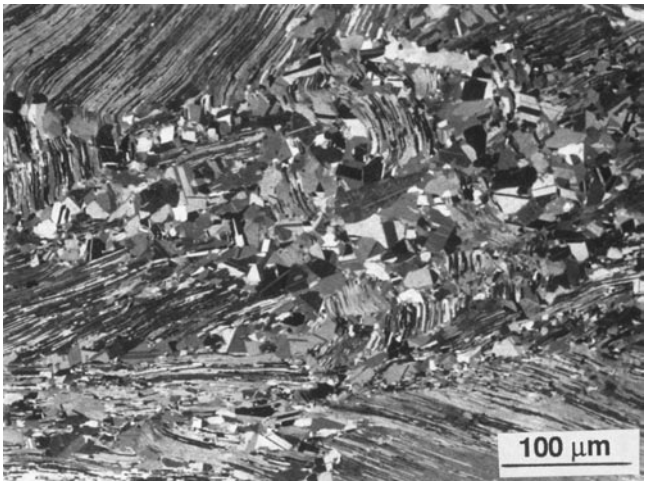

Fig. 1—Polarized-light optical microstructure of as-conventionally forged Ti-45Al-2Cr-2Nb (at. pct).

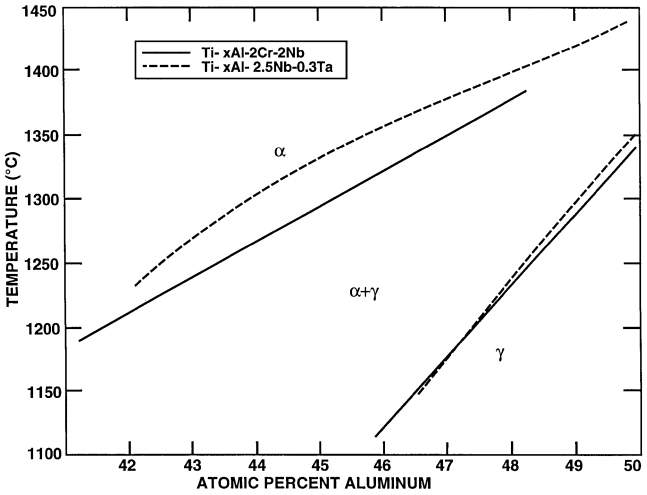

Fig. 2—Portions of the Ti-*x*Al-2Cr-2Nb and Ti-*x*Al-2.5Nb-0.3Ta (at. pct) pseudobinary phase diagrams showing the alpha transus and gamma solvus lines.

II. MATERIALS AND EXPERIMENTAL PROCEDURES

A. *Materials*

The material used in the major part of the present investigation was the near-gamma titanium aluminide alloy Ti-45Al-2Cr-2Nb. Its measured composition (in at. pct) was 50.9 titanium, 44.9 aluminum, 1.97 chromium, and 2.00 niobium. Interstitial levels (in wt ppm) were measured as 539 oxygen, 75 nitrogen, 100 carbon, and 17 hydrogen. The material was received in the form of cast–plus–hot-isostatically pressed induction-skull melted ingots 70 mm in diameter, which had been produced by the Duriron Company (Dayton, OH). Mults were cut from the ingots, encapsulated in stainless steel cans, and conventionally forged to a 60 pct height reduction at a temperature of 1200 °C and an effective strain rate of approximately 0.2 s^{-1} using the 1000-ton Erie forging press located at the Wright Laboratory Materials Directorate (Wright-Patterson Air Force Base, OH). Details on the forging process are contained in Reference 3. The as-forged microstructure comprised regions of both fine, globularized structure with gamma and alpha-two grains as well as remnant, deformed lamellar colonies (Figure 1). As will be discussed later, subsequent subtransus heat treatment led to a uniform microduplex structure with no noticeable microsegregation. This material was used in the detailed heat-treatment studies described in Section II–B.

To obtain material for demonstrating the feasibility of scaling-up the heat treatments developed in this work, cylinders were electric-discharge machined from the conventionally forged Ti-45.Al-2Cr-2Nb cylinders and then isothermally forged by the Ladish Company (Cudahy, WI) to a subscale disk geometry of approximately 102 mm in diameter with section thicknesses ranging from approximately 8 mm (web areas) to 19 mm (ribs). A larger isothermal forging of similar composition (Ti-46.7Al-2.01Cr-2.03Nb) was provided by General Electric Aircraft Engines (Evendale, OH) to further establish the feasibility of heat-treatment process scaleup. This forging was also of a disk-like geometry, with a diameter of 250 mm and section thickness varying from 19 to 46 mm.

The alpha transus temperatures of the two program materials were determined by a series of heat treatments followed by optical metallography; these transus temperatures were found to be 1290 °C for the Ti-45Al-2Cr-2Nb material and 1340 °C for the Ti-46.7Al-2Cr-2Nb alloy. The accuracy of the transus temperatures was verified by determining the volume fraction of undissolved gamma phase at several temperatures below the transus. Use of the inverse lever rule and the pseudobinary phase diagram for Ti-*x*Al-2Cr-2Nb,[3] reproduced in Figure 2, in conjunction with the volume fraction measurements, enabled transus determinations within approximately ±2 °C.

B. *Experimental Procedures*

The experimental work consisted of a variety of heat-treatment studies on small samples of the Ti-45Al-2Cr-2Nb alloy and on the isothermal forgings of both the Ti-45Al-2Cr-2Nb and Ti-46.7Al-2Cr-2Nb alloys. All heat treatments were conducted in large laboratory furnaces of considerable thermal mass in order to avoid furnace temperature changes during sample insertion.

Heat treatment of small samples of Ti-45Al-2Cr-2Nb was conducted to establish the kinetics of gamma phase dissolution and alpha grain growth during supertransus heat treatment. For this purpose, a series of cubes (with edge lengths of approximately 11.4 mm) were machined from the midheight of the decanned forgings. Care was taken to extract material only from a given radial location as well (*viz.*, the midradius), to ensure a uniform composition in all samples and, thus, to avoid possible variations in heat-treatment response due to center-to-surface macrosegregation.[3] Heat treatment comprised a two-step process consisting of an initial step in a furnace operating at a temperature between $T_\alpha - 20$ °C and $T_\alpha - 5$ °C. The initial step, lasting 30 minutes, served to complete the globularization of the wrought, conventionally forged material and to produce, thereby, a relatively uniform structure of alpha grains pinned by gamma particles prior to the second step of treatment. The second step lasted between 30 seconds and 5 minutes, or for times that were found to be sufficient to dissolve the remnant gamma particles from the first step of

treatment as well as to bring about substantial grain growth subsequent to the gamma particle dissolution. Following the second step, all samples were water quenched. Optical metallography using polarized light illumination and scanning electron microscopy using backscattered electron imaging on polished sections were utilized to determine the microstructures developed by the heat treatments. These observations were interpreted using the models described in Section III.

In a parallel series of experiments, several 26-mm cubes were sectioned from the Ti-45Al-2Cr-2Nb forgings and heat treated to establish an emissivity value that could be used to model the temperature transients that pertained to the transfer portion of the previous two-step treatments. This work consisted of heating each cube in a fashion identical to that used in the first step of heat treatment, removing it from the furnace, and recording the cooling curve for the sample using a two-color infrared pyrometer sighted on one of the flat faces of the cube. The pertinent emissivity value was established by fitting the measured cooling curves with ones predicted from a simple radiation cooling analysis described in Section III.

Two-step furnace heat treatments were also conducted (in a similar manner to those used for the small samples) on the small Ti-45Al-2Cr-2Nb and the large Ti-46.7Al-2Cr-2Nb isothermal forgings to establish process scaleup feasibility. An additional preheat step at 925 °C was incorporated to avoid thermal shock and the possible fracture that might occur upon charging low-ductility gamma titanium aluminide material directly into a furnace operating at a temperature on the order of 1300 °C. After heat treatment, the forgings were air cooled to induce lamellar transformation of the high-temperature alpha phase. They were then sectioned and prepared for optical metallography (as-polished condition) and macrophotography (polished-and-etched condition).

III. ANALYSIS METHODS

The experimental data were analyzed and interpreted using models for the temperature transients during the transfer stage of the two-step heat-treatment process, interface reaction–controlled or diffusion-controlled dissolution of second-phase particles, and grain growth in the presence or absence of second-phase particles. These analyses are summarized in the following subsections.

A. *Temperature-Transient Analysis*

The temperature transients during the transfer of small samples from a subtransus furnace to a supertransus furnace were analyzed using the simple radiation equation for the homogeneous cooling/heating of a cube whose edge length is l,[13] *i.e.*,

$$dT_s = (6e\sigma/\rho cl)\left(T_E^4 - T_s^4\right) d\mathrm{t} \qquad [1]$$

in which $T_s(t)$ is the sample temperature as a function of time, $e \equiv$ emissivity, $\sigma \equiv$ the Stefan–Boltzmann constant, $\rho \equiv$ sample density, $c \equiv$ specific heat, and $T_E \equiv$ environment temperature. The adequacy of the uniform heating assumption was verified through calculation of the inverse Biot number ($\mathrm{Bi}^{-1} \gtrsim 6$, in the present case) and reference to Heisler diagrams[13,14] for the estimation of the maximum temperature nonuniformity. The surface-to-center temperature nonuniformity for the 11.4-mm Ti-45Al-2Cr-2Nb cubes was estimated to be on the order of 1.5 °C or less.

Input property data for the application of Eq. [1] were as follows: $e = 0.60$ (from fitting of the cooling curve data for the 26-mm Ti-45Al-2Cr-2Nb cubes), $\rho = 3.98 \times 10^{-3}$ g/mm^3, $c = 1.00$ Ws/gK (measured data for the Ti-45Al-2Cr-2Nb alloy at $T \approx T_\alpha$ in Reference 15), and $l = 11.4$ mm. Eq. [1] was utilized to calculate both the initial temperature *drop* when samples were removed from the subtransus furnace ($T_E \equiv$ ambient = 298 K) as well as the subsequent temperature rise when samples were placed in the supertransus furnace ($T_E \equiv$ temperature of the supertransus furnace).

B. *Gamma Particle Dissolution: Interface Reaction Kinetics*

Previous work on the homogenization of a banded near-gamma titanium aluminide alloy (Ti-46.6Al-2.5Nb-0.3Ta, at. pct) in the single-phase alpha field suggested that gamma phase dissolution is controlled by a second-order interface reaction.[16] Hence, the dissolution of gamma particles during supertransus heating of the Ti-45Al-2Cr-2Nb alloy in the present investigation was interpreted using the (second-order) interface reaction kinetics approach discussed by Aaron and Kotler[17] and Semiatin and McQuay.[16]

Assuming uniform, spherical gamma particles of a radius r_γ, the time rate of dissolution $r_\gamma(t)$ is given by the following relation:

$$dr_\gamma/d\mathrm{t} = -A_2\,\{T^2 \exp(-Q/\mathrm{R}T)\}\,\{\Delta C_k/C_s\}^2 \qquad [2]$$

in which A_2 is a rate constant, T is absolute temperature, Q is an activation energy for the process, and R is the gas constant. The definitions of ΔC_k and C_s are shown in Figure 3(a). The concentration difference (ΔC_k) is the difference between the maximum allowable solute concentration in the matrix (alpha phase, in the present case), C_s, and the instantaneous concentration of the matrix phase C_α, *i.e.*, $\Delta C_k \equiv C_s - C_\alpha$. In the current work, the solute concentration was taken to be the aluminum concentration, and the pseudobinary phase diagram (Figure 2) was used.

Denoting the instantaneous volume fractions of the alpha and gamma phases by f_α and f_γ, respectively, the solute concentration in the gamma phase by C_γ, and the overall alloy concentration by C_0, a mass balance gives the following relations:

$$C_0 = f_\alpha C_\alpha + f_\gamma C_\gamma = (1 - f_\gamma) C_\alpha + f_\gamma C_\gamma \qquad [3a]$$

or

$$C_\alpha = (C_0 - f_\gamma C_\gamma)/(1 - f_\gamma) \qquad [3b]$$

Furthermore, denoting the number of gamma particles per unit volume by N_γ (assumed to be a fixed quantity during the dissolution process), a relation between r_γ, f_γ, and N_γ is obtained:

$$f_\gamma = (4\ \pi N_\gamma/3) r_\gamma^3 \qquad [4]$$

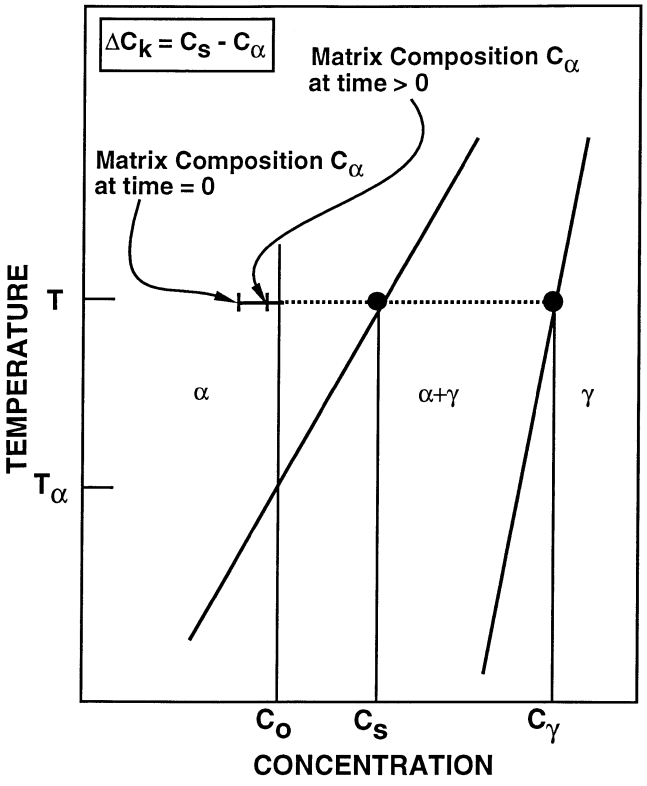

Fig. 3—Schematic illustrations and nomenclature used in the modeling of second-phase dissolution controlled by (*a*) interface reaction–controlled kinetics or (*b*) diffusion-controlled kinetics.

Inserting the definition for ΔC_k and Eqs. [3b] and [4] into Eq. [2], the following differential equation for $r_\gamma(t)$ is obtained:

$$dr_\gamma/dt = -\left(A_2/C_s^2\right)\{T^2 \exp(-Q/RT)\} \cdot \left\{C_s - \frac{3C_0 - 4\pi N_\gamma C_\gamma r_\gamma^3}{3 - 4\pi N_\gamma r_\gamma^3}\right\}^2 \quad [5a]$$

or

$$dr_\gamma/dt = -F(T)\left\{C_s - \frac{3C_0 - 4\pi N_\gamma C_\gamma r_\gamma^3}{3 - 4\pi N_\gamma r_\gamma^3}\right\}^2 \quad [5b]$$

Equation [5b] is a relatively simple differential equation that can be integrated to obtain gamma particle dissolution kinetics at specific temperatures (and, hence, values of $F(T)$, C_s, and C_γ), provided the rate constant A_2 is known.

The rate constant A_2 was determined through the analysis of dissolution kinetics measurements for the homogenization of the banded microstructure in the Ti-46.6Al-2Nb-0.3Ta alloy; these measurements were summarized in Reference 16. This analysis required an expression similar to Eq. [5], but modified for the different (planar) geometry of the gamma phase in the banded microstructure. Assuming that the gamma grain bands are flat slabs of a thickness h_γ with a center-to-center spacing of H, the corresponding differential equation for this latter geometry is easily derived. It is the following:

$$dh_\gamma/dt = -2F(T)\left\{C_s - \frac{C_0 - (h_\gamma/H)C_\gamma}{1 - (h_\gamma/H)}\right\}^2 \quad [6]$$

The integration of Eq. [6] for specific values of temperature T (and, hence, C_s and C_γ), coupled with measured values of the dissolution time (*i.e.*, time at which $h_\gamma = 0$), enabled the determination of the rate constant A_2. For this purpose, the pseudobinary phase diagram measured by Semiatin and McQuay[18] for Ti-*x*Al-2.5Nb-0.3Ta (reproduced in Figure 2) was used to obtain the pertinent values of C_s and C_γ needed for the analysis. An activation energy of 312 kJ/mol[19] was used in the majority of the calculations. Other values for Q (*e.g.*, 160 kJ/mol) were also used, but did not substantially change the overall interpretation of the predicted *vs* measured gamma particle dissolution behaviors discussed in Section IV.

C. *Gamma Particle Dissolution: Diffusion-Controlled Kinetics*

Because the gamma particles were found as a fine, apparently incoherent phase in the present heat treatments, unlike the apparently coherent gamma phase that was present during the previous homogenization work,[16] the experimental results were also interpreted in the context of diffusion-controlled dissolution kinetics. Because of the small volume fraction and fine scale of the gamma particles relative to the much larger alpha grain size, the assumptions of the Whelan ''spherical-infinite'' dissolution model[20] were met to a good approximation. Thus, this model was used for the diffusion analysis. The nomenclature of the Whelan model is shown in Figure 3(b). Using terminology similar to that for the interface reaction model, the diffusion-controlled dissolution model postulates a gamma particle of fixed composition C_γ and initial radius r_{γ_0} dissolving into the surrounding (alpha) matrix, whose composition varies from a maximum value of C_s (dictated by the phase diagram) at the particle-matrix interface to a value of C_e, or the initial solute concentration distant from the particle. Neglecting the compositional dependence of the interdiffusion coefficient $\tilde{D}$, the time for complete dissolution (t_d) is given by the expression

$$\ln \tau_c = (-2/\psi) \arctan \psi \quad [7]$$

in which

$$\tau_c = \left(2\tilde{D}t_d/r_{\gamma_0}^2\right)(C_s - C_e)/(C_\gamma - C_s) \quad [8a]$$

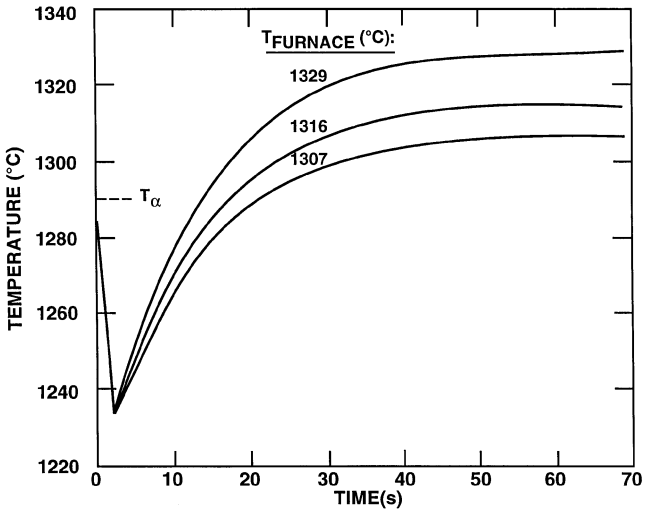

Fig. 4—Predicted temperature transients experienced by 11.4-mm Ti-45Al-2Cr-2Nb cubes during transfer from a furnace operating at $T_\alpha - 5$ °C (1285 °C) to a furnace at a supertransus temperature of $T_\alpha + 17$ °C (1307 °C), $T_\alpha + 26$ °C (1316 °C), or $T_\alpha + 39$ °C (1329 °C).

$$\psi = \sqrt{1 - p^2}/p \qquad [8b]$$

and

$$p = \{(C_\gamma - C_e)/2\pi(C_\gamma - C_s)\}^{1/2} \qquad [8c]$$

A value of C_e equal to 44.8 at. pct was used in the calculations for the supertransus heat treatment of the Ti-45Al-2Cr-2Nb alloy. This aluminum concentration lies between the value of C_α, corresponding to an initial subtransus heat treatment at $T_\alpha - 5$ °C (*i.e.*, $C_\alpha = 44.7$ at. pct), and the overall aluminum content of the alloy (44.9 at. pct).

D. *Grain growth analysis*

Grain growth during the supertransus portion of the two-step heat treatment was analyzed using the general approach discussed by Grewal and Ankem[21,22,23] and Anderson and Grong,[24] which has previously been applied specifically to the gamma titanium aluminide alloys by Seetharaman and Semiatin.[25] Based on these previous efforts, alpha grain growth in the presence of stable or dissolving second-phase gamma particles can be described by the following relation:

$$dD_\alpha/dt = k^*\left[(1/D_\alpha) - \left(1/D_\alpha^L\right)\right]^{p-1} \qquad [9]$$

in which D_α (t) denotes the alpha grain size as a function of time, $k^* = k^*$ (T) is a rate constant, D_α^L is the limiting alpha grain size, and p is the grain growth exponent. Various models for the effect of pinning particles on the limiting alpha grain size have been proposed. These models include the early treatment by Zener[26] and, later, more refined analytical and numerical approaches by Hellman and Hillert[27] and Hazzledine and Oldershaw,[28] for example. Denoting the gamma particle diameter by d_γ, results for each of these investigations are as follows:

$$D_\alpha^L/d_\gamma = 0.667\, f_\gamma^{-1} \text{ (Zener)} \qquad [10a]$$

$$D_\alpha^L/d_\gamma = 1.817\, f_\gamma^{-1/3} \text{ (Hellman and Hillert)} \qquad [10b]$$

and

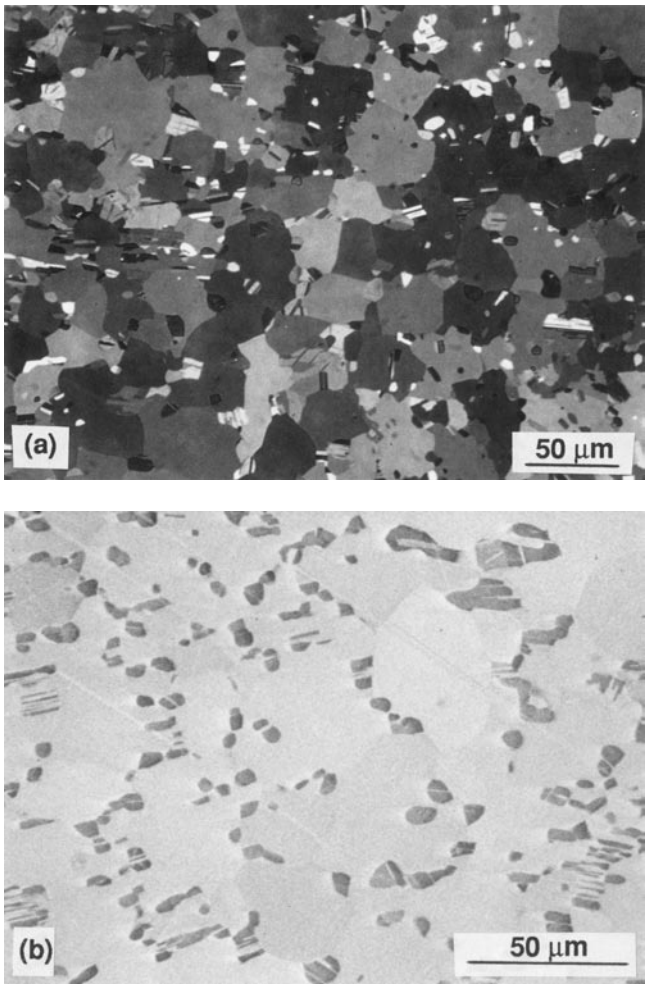

Fig. 5—Microstructure developed in a 11.4-mm Ti-45Al-2Cr-2Nb cube after a subtransus heat treatment at $T_\alpha - 5$ °C (1285 °C) for 30 min followed by water quenching: (*a*) polarized-light optical microstructure and (*b*) backscattered electron micrograph. In the latter photograph, the dark phase is gamma and the lighter phase is alpha-two.

$$D_\alpha^L/d_\gamma = 2.8\, f_\gamma^{-1/3} \text{ (Hazzledine and Oldershaw)} \qquad [10c]$$

It should be noted that the Zener model generally applies to situations involving small volume fractions (*e.g.*, $f_\gamma \lesssim 0.01$) of fine particles located randomly at the grain boundaries. For situations involving higher volume fractions of particles distributed in a nonrandom manner, the other two models have been found to provide a better representation of observed behaviors.

Equation [9] is easily integrated *via* numerical techniques if the values of k^* and D_α^L are known. For a dissolving second phase, D_α^L can be a function of time. In the case of a distribution of uniform size, spherical gamma particles which dissolve uniformly such that the number per unit volume N_γ remains constant, the exact functional dependence is readily found by combining Eqs. [4] and [10], yielding the following:

$$D_\alpha^L = (1/\pi N_\gamma) r_\gamma^{-2} \text{ (Zener)} \qquad [11a]$$

$$D_\alpha^L = (36/\pi N_\gamma)^{1/3} \text{ (Hellman and Hillert)} \qquad [11b]$$

$$D_\alpha^L = (132/\pi N_\gamma)^{1/3} \text{ (Hazzledine and Oldershaw)} \qquad [11c]$$

Equations [11b] and [11c] reveal that D_α^L is predicted to be

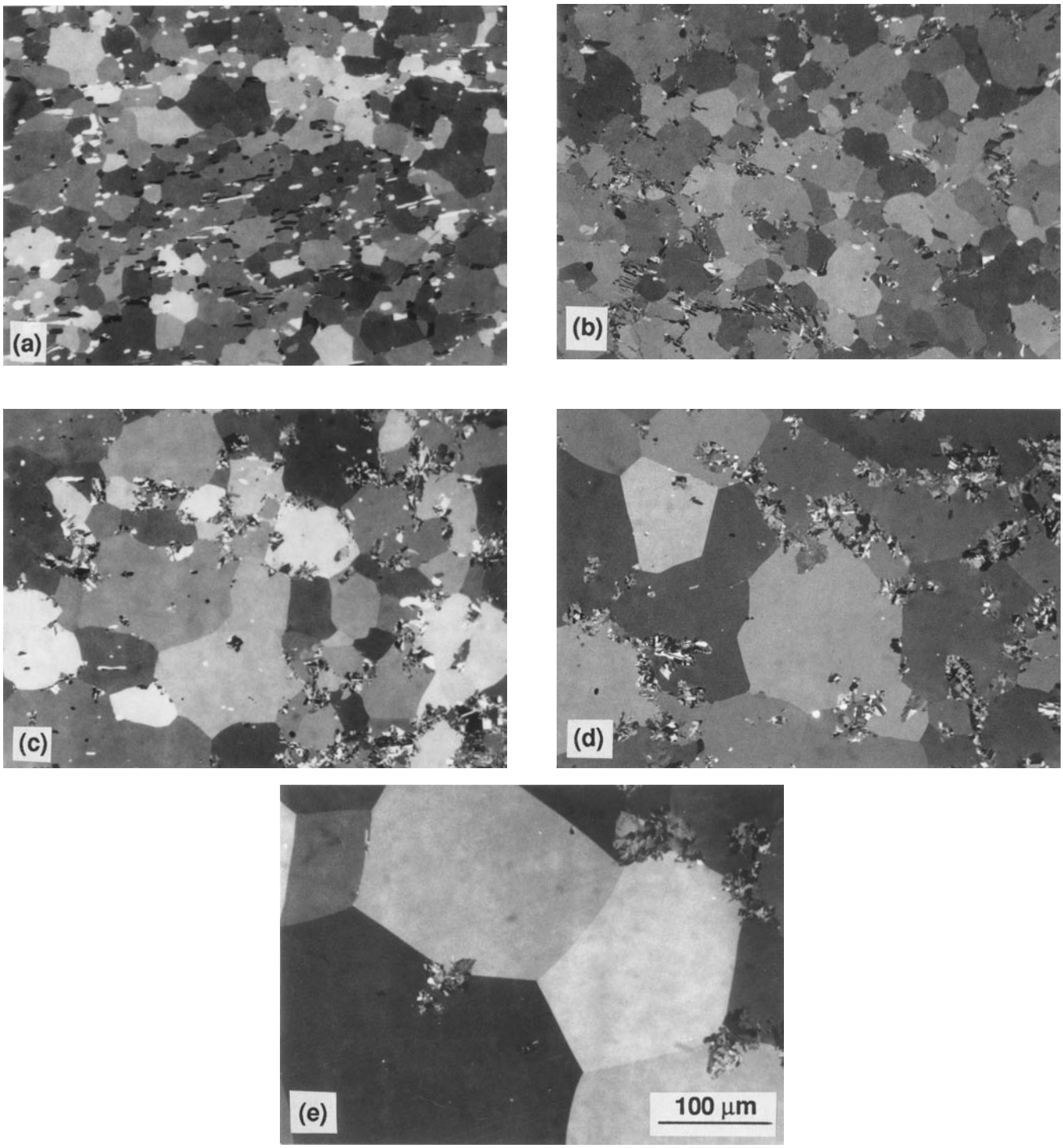

Fig. 6—Polarized-light optical microstructures developed in 11.4-mm Ti-45Al-2Cr-2Nb cubes after a subtransus heat treatment at $T_\alpha - 5$ °C (1285 °C) for 30 min followed by a supertransus heat treatment at $T_\alpha + 17$ °C (1307 °C) for times of (*a*) 60 s, (*b*) 90 s, (*c*) 120 s, (*d*) 180 s, and (*e*) 300 s. Following the supertransus heat treatment, all samples were water quenched.

constant for constant N_γ by the latter two models. The implication of this result for the present investigation is that the use of a suitably long subtransus heat treatment which leads to a stable alpha grain size ($D_\alpha = D_\alpha^L$) may give rise to negligible alpha grain growth while gamma particles dissolve during subsequent supertransus heating.

For the case in which all of the second phase has dissolved, Eq. [9] can be integrated directly to yield the classical grain growth relation for a single-phase alloy:

$$D_\alpha^p - D_{\alpha_0}^p = k^* p (t - t_0) \qquad [12]$$

in which $D_\alpha (t_0) = D_{\alpha_0}$.

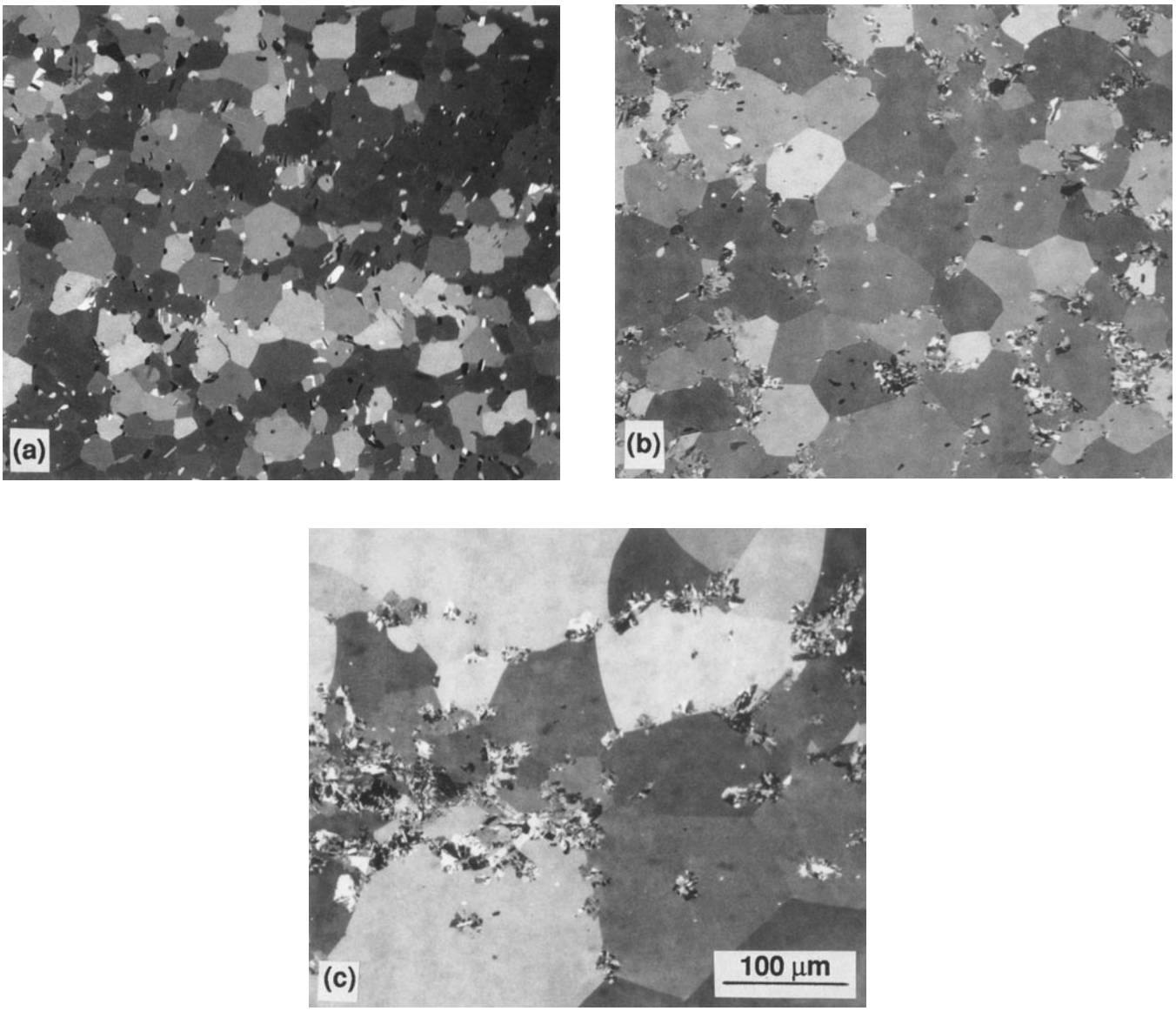

Fig. 7—Polarized-light optical microstructures developed in 11.4-mm Ti-45Al-2Cr-2Nb cubes after a subtransus heat treatment at T_α − 5 °C (1285 °C) for 30 min followed by a supertransus heat treatment at T_α + 39 °C (1329 °C) for times of (*a*) 45 s, (*b*) 60 s, and (*c*) 90 s. Following the supertransus heat treatment, all samples were water quenched.

IV. RESULTS AND DISCUSSION

The results of this investigation are presented and discussed in the following four subsections, which address temperature transients during heat treatment, dissolution kinetics for second-phase particles, alpha grain growth kinetics, and heat-treatment scaleup/process validation.

A. *Temperature Transients during Heat Treatment*

The temperature transients experienced by the small 11.4-mm Ti-45Al-2Cr-2Nb cubes during transfer from a furnace at a subtransus temperature to a furnace at a supertransus temperature were calculated using Eq. [1]. The results of these calculations for a subtransus temperature of 1285 °C (T_α − 5 °C) and supertransus temperatures of 1307 °C, 1316 °C, and 1329 °C (T_α + 17 °C, T_α + 26 °C, and T_α + 39 °C) are shown in Figure 4. In all three cases, the (measured) transfer time has been taken to be 2 seconds. During this transfer, a substantial temperature drop (approximately 60 °C) is predicted to occur, but the samples quickly recover this loss upon being placed in the supertransus furnace. However, the heating time for the sample to achieve the supertransus furnace temperature is non-negligible. In each case, approximately 30 seconds is predicted to be required for the sample to reach a temperature 10 °C below the supertransus furnace temperature, and approximately 35 seconds is required for it to be within 5 °C of the supertransus furnace temperature. The effect of these transients on gamma particle dissolution kinetics and alpha grain growth was taken into account in an approximate manner, as described subsequently.

B. *Dissolution Kinetics for Second-Phase Particles*

The dissolution kinetics for the second-phase (gamma) particles during the supertransus heat treatments of Ti-

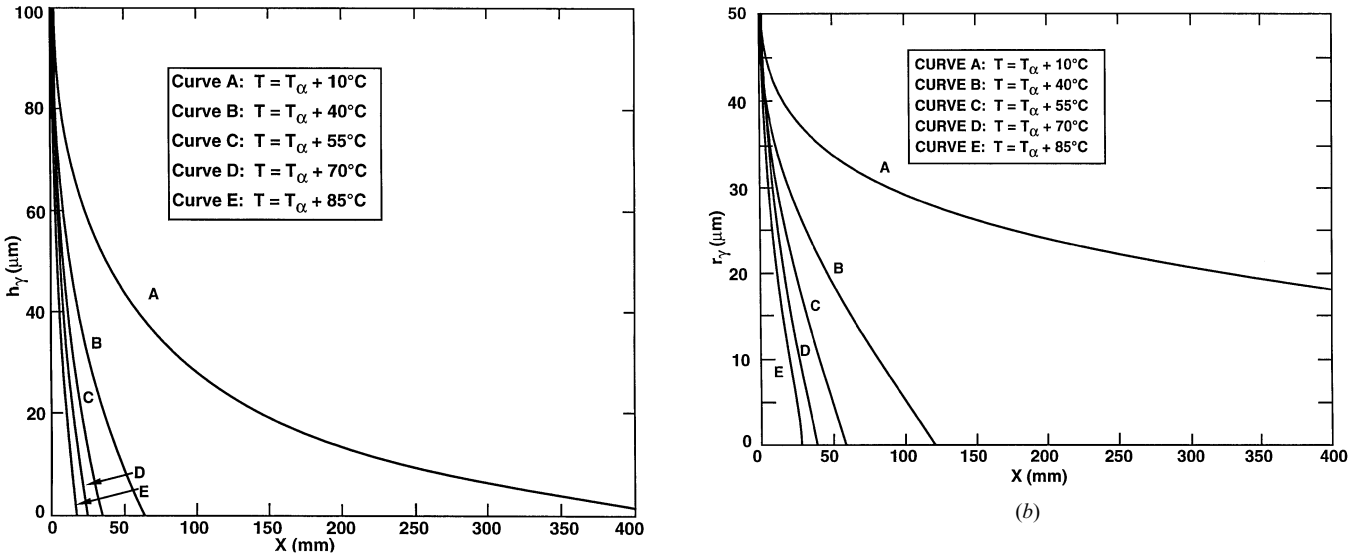

(*a*) (*b*)

Fig. 8—Predicted interface reaction–controlled dissolution kinetics for gamma phase segregate in Ti-46.6Al-2.5Nb-0.3Ta homogenized at various temperatures in the alpha phase field. Prior to homogenization, the volume fraction of gamma was assumed to be 50 pct in the form of (*a*) 100-μm-thick bands (slabs) or (*b*) 100-μm-diameter spherical particles.

45Al-2Cr-2Nb were determined experimentally by comparing the microstructures developed in the subtransus heat treatments to those from the supertransus heat treatments. Figure 5 shows an example of the microstructure obtained through subtransus heat treatment at 1285 °C (T_α − 5 °C) for 30 minutes followed by water quenching. By and large, the structure consists of equiaxed alpha-two grains (approximately 30 μm in size) pinned by approximately 6 vol. pct of 5-μm-diameter gamma particles. This value of alpha grain size is very close to that predicted from Eq. [10c] (*i.e.*, $D_\alpha^L = 36$ μm) for $d_\gamma = 5$ μm and $f_\gamma = 0.06$.

Examples of microstructures from samples which were supertransus heat treated following a subtransus heat treatment at 1285 °C (T_α − 5 °C) for 30 minutes are shown in Figures 6 and 7. In both figures, the microstructures for the shorter time heat treatments exhibit residual gamma particles, while the longer time treatments reveal structures without gamma particles and consisting of essentially equiaxed alpha-two grains with patchy regions of feathery or massive gamma. (As has been shown previously,[29] these forms of gamma are transformation products produced during rapid cooling from the alpha phase field.) Micrographs such as those shown in Figures 6 and 7 revealed that the times to dissolve the gamma particles remaining after a subtransus heat treatment at T_α − 5 °C were 85, 60, or 45 seconds for supertransus treatments at T_α + 17 °C, T_α + 26 °C, or T_α + 39 °C, respectively. Because these are total heating times in the supertransus furnace and include transient heating effects such as those shown in Figure 4, the actual dissolution times were shorter. Because the primary interest here is in order-of-magnitude estimates of the dissolution kinetics, the approximate dissolution times *at temperature* were taken to be the total furnace time minus 30 seconds, as suggested by the results in Figure 4. For heating at the three supertransus temperatures, the approximate dissolution times (at temperature) were thus taken to be 55, 30, and 15 seconds. These measured times for gamma particle dissolution are now compared to theoretical predictions from interface reaction–controlled and diffusion-controlled models.

1. *Interface reaction–controlled kinetics*

As mentioned in Section III–B, the approach taken to predict the dissolution times, assuming an interface reaction model, comprised, first, the determination of a rate constant (from the homogenization data for Ti-46.6Al-2.5Nb-0.3Ta in Reference 16) and, second, the application of a similar analysis for predicting the dissolution kinetics of the spherical gamma particles observed in the present heat-treatment study on Ti-45Al-2Cr-2Nb.

The results of the rate constant determination are summarized in Figure 8 and Table I. Figure 8(a) shows the calculated dissolution kinetics derived from Eq. [6] using values of C_0, C_s, C_γ, h_γ ($t = 0$), and H (listed in Table I) for the specific heat treatments of Reference 16. The plots are in terms of h_γ (t) *vs* the variable X, defined as the following:

$$X \text{ (mm)} \equiv t \cdot F(T) = t \cdot \left(A_2/C_s^2\right) \{T^2 \exp(-Q/RT)\} \quad [13]$$

At complete dissolution, $h_\gamma = 0$, $X = X_d$, and the rate constant A_2 is determined simply from the measured dissolution time $t = t_d$, the calculated value of X_d (Figure 8(a)), and the application of Eq. [13]. These estimates of A_2 are listed in Table I under the column for ''banded microstructure.'' They show a variation of about a factor of 2 for the various homogenization experiments, a variation which is considered to be reasonable in view of the almost 100-fold variation in measured dissolution times.

The assumption of a banded, or planar, geometry for the gamma-phase microconstituent in the Ti-46.6Al-2.5Nb-0.3Ta homogenization experiments becomes increasingly poor as the volume fraction of remnant gamma goes to zero. In these cases, the remnant gamma phase takes on more of a spherical geometry. To assess such a geometry

Table I. Homogenization Kinetics Results for Ti-46.6Al-2.5Nb-0.3Ta (Atomic Percent)

Temperature* (°C)	C_s (At. Pct)	C_γ (At. Pct)	Measured Dissolution Time, t_d (s)	Banded Microstructure**		Spherical Particles†	
				X_d (mm)	A_2 (mm/s K^2)	X_d (mm)	A_2 (mm/s K^2)
T_α + 10	47.0	50.5	18,000	456.2	17.42	1,416.6	54.10
T_α + 40	48.2	51.5	2,700	64.5	11.06	121.3	20.79
T_α + 55	49.0	52.0	1,080	34.3	12.23	57.9	20.64
T_α + 70	49.6	52.5	480	23.5	15.60	38.1	25.29
T_α + 85	50.2	53.0	240	17.2	18.96	27.0	29.76

*T_α = 1360 °C = 1633 K.
**Banded microstructure with H = 200 μm, h_γ (t = 0) = 100 μm.
†Microstructure with spherical gamma grains, r_γ (t = 0) = 50 μm, $N_\gamma = 9.6 \times 10^{-7}$ μm^{-3}.

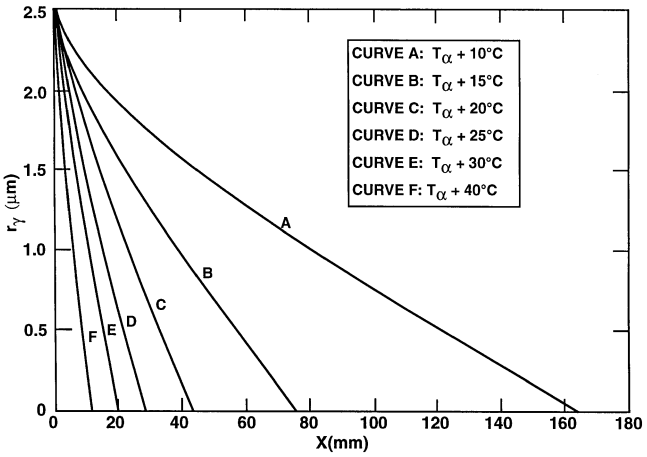

Fig. 9—Predicted interface reaction–controlled dissolution kinetics for gamma phase particles in Ti-45Al-2Cr-2Nb during supertransus heat treatment at various temperatures. Prior to the supertransus heat treatment, the microstructure was assumed to contain 6 vol pct of 5-μm-diameter spherical particles.

effect, simulations similar to those for the planar geometry were conducted using Eq. [5], assuming a spherical microconstituent with an initial volume fraction identical to that of the previous calculations (*i.e.*, 50 pct). The results of these calculations are summarized in Figure 8(b) and Table I. The rate constant A_2 in these cases was estimated to be approximately twice that derived for the planar geometry.

The dissolution time for the gamma particles in Ti-45Al-2Cr-2Nb during supertransus heat treatment was then predicted from the rate constant (A_2) determined from the homogenization data and additional dissolution simulations (similar to those described previously) carried out by numerical integration of Eq. [5]. Sample simulation results from these efforts are shown in Figure 9 (r_γ *vs* X) and Table II (X_d). By applying Eq. [13] as before, the values of X_d were used to estimate the dissolution time t_d. These predicted dissolution times are compared to the measured values in Table II. The predictions are seen to *exceed* the measurements by approximately one or two orders of magnitude.

2. *Diffusion-controlled kinetics*

Estimates of the time for the dissolution of gamma particles during supertransus heat treatment of Ti-45Al-2Cr-2Nb were also obtained using the diffusion-controlled kinetics embodied in the Whelan spherical-infinite model (Eq. [7]). For this purpose, approximate values of the diffusivity $\tilde{D}$ were obtained from the data of Sprengel *et al.*[19] for the alpha-two phase in the binary titanium-aluminum system. In this work, the diffusivity was determined to be $\tilde{D}$ (mm^2/s) = 10^3 exp ($-37{,}545/T$(K)). Predicted dissolution times based on diffusion-controlled kinetics and diffusivities from this relation were found to be comparable to the measured values (Table III). It is also important to note that the ratio of the predicted dissolution times from the diffusion analysis for the three temperatures in the table (124:70:34 = 3.65:2.06:1.00) is almost exactly the same as the measured ratio (55:30:15 = 3.67:2.00:1.00), lending further credence to the applicability of diffusion-dominated kinetics. By contrast, the interface reaction kinetics model predicts an approximately sevenfold variation in dissolution time for the highest and lowest of the three supertransus heat-treatment temperatures (Table II), or twice the variation actually observed.

The agreement between the diffusion model predictions and the experimental observations must still be viewed as somewhat qualitative in nature, because $\tilde{D}$ data for the ordered alpha-two phase, rather than the disordered alpha phase, were used. It is likely that $\tilde{D}$ for disordered alpha would be higher than that for ordered alpha-two. This would *decrease* the predicted dissolution times, a trend that would tend to make agreement between the measured and predicted dissolution times in Table III better. On the other hand, the niobium and chromium solutes in the Ti-45Al-2Cr-2Nb alloy would tend to lower the diffusivity, and would thus tend to give rise to longer predicted dissolution times. However, the exact quantitative magnitude of each of these effects cannot be gaged until additional diffusivity data are obtained.

C. *Alpha Grain Growth Kinetics*

The ''short-time'' alpha grain growth kinetics measured in the present work for Ti-45Al-2Cr-2Nb (Figure 10) are readily interpreted in terms of previous models of grain boundary pinning by second-phase particles[26,27,28] and the ''long-time'' alpha grain growth kinetics reported previously.[25] As mentioned in Section III–D, negligible alpha grain growth prior to completion of dissolution would be expected if the gamma particles were of equal size and dissolved uniformly. This indeed was observed; the alpha grain size measurements for supertransus heating at various temperatures following a subtransus soak at $T_\alpha - 5$ °C were all approximately equal to that established during the subtransus step (≈35 μm), at least within experimental error (Figure 10).

Following the completion of gamma particle dissolution,

Table II. Interface Reaction–Controlled Dissolution Kinetics during Supertransus Heat Treatment of Ti-45Al-2Cr-2Nb (Atomic Percent)*

Temperature** (°C)	C_s (At. Pct)	C_γ (At. Pct)	X_d (mm)	Predicted Dissolution Time, t_d (s)		Measured Dissolution Time, t_d (s)
				A_2 = 15.05 mm/s K²	A_2 = 30.12 mm/s K²	
T_α + 17	45.5	49.4	62.6	7205	3600	55
T_α + 26	45.8	49.55	26.4	2660	1330	30
T_α + 39	46.3	49.8	12.1	1015	505	15

*Heat treatment consisting of T_α − 5 °C/30 min + supertransus treatment at temperatures indicated.
**T_α = 1290 °C.

Table III. Diffusion-Controlled Dissolution Kinetics during Supertransus Heat Treatment of Ti-45Al-2Cr-2Nb (Atomic Percent)*

Temperature** (°C)	r_{γ_0} (μm)	C_e (At. Pct)	C_s (At. Pct)	C_γ (At. Pct)	Predictions		Measured Dissolution Time, t_d (s)
					$\tilde{D}t_d$ (mm²) (Eq. [7])	t_d (s)	
T_α + 17	2.5	44.8	45.5	49.4	5.92 × 10⁻⁶	124	55
T_α + 26	2.5	44.8	45.8	49.55	3.86 × 10⁻⁶	70	30
T_α + 39	2.5	44.8	46.3	49.8	2.28 × 10⁻⁶	34	15

*Heat treatment consisting of T_α − 5 °C/30 min + supertransus treatment at temperatures indicated.
**T_α = 1290 °C.

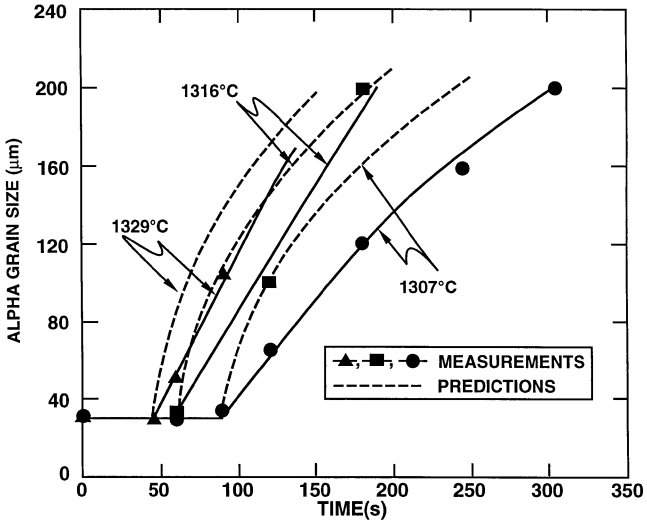

Fig. 10—Measured grain growth kinetics for Ti-45Al-2Cr-2Nb heat treated at T_α − 5 °C (1285 °C) for 30 min followed by supertransus heating at supertransus temperatures of T_α + 17 °C (1307 °C), T_α + 26 °C (1316 °C), and T_α + 39 °C (1329 °C). The measured grain growth data are compared to predictions based on longer time grain growth kinetics.[25]

the alpha phase exhibited a very rapid rate of grain growth (Figure 10). These measured grain growth rates are compared to predictions based on a previous fit to long-time data (t = 120 to 3600 seconds) obtained on Ti-45Al-2Cr-2Nb at 1321 °C (1594 K) by Seetharaman and Semiatin.[25] The analytical fit extracted from this earlier effort (using a simple Arrhenius correction for the grain-growth rate constant) is the following:

$$D_\alpha^p - D_{\alpha_0}^p = 1302 \cdot \left\{ \exp\left[\frac{Q}{\mathrm{R}} \cdot \left(\frac{1}{1594} - \frac{1}{T} \right) \right] \right\} \{ t - t_0 \} \quad [14]$$

in which D_α (t) and D_{α_0} denote the instantaneous and initial grain sizes in μm; $p \equiv$ the grain growth exponent (= 2.26); $Q \equiv$ activation energy, taken here to be 312 kJ/mol[19] (although the precise value has only a small quantitative effect for temperatures close to 1594 K); R ≡ the gas constant; $T \equiv$ absolute temperature; and D_α ($t = t_0$) = D_{α_0}. Here, D_{α_0} is assumed to be 35 μm, and t_0 is taken to be the time at which gamma particle dissolution is completed, *i.e.*, the time at which marked alpha grain growth was noted. Comparison of the measured grain growth results and those predicted based on the previous long-time observations show reasonable first-order agreement (Figure 10).

D. *Heat-Treatment Scaleup/Process Validation*

Heat-treatment cycles for the small and large isothermal forgings established the feasibility of applying a short-time supertransus heat-treatment technique to obtain moderately fine alpha grain sizes.

The smaller Ti-45Al-2Cr-2Nb forging (subscale disk) represented a case for which a relatively uniform temperature throughout the part could be maintained upon charging from a subtransus furnace into a supertransus furnace. The high degree of temperature uniformity was ascertained by reference to the Heisler diagrams for plate geometries[13,14] as well as finite-element method (FEM) simulations of the heating process, both of which suggested maximum temperature nonuniformity of approximately 2 °C (except at the extremities of the ribs). Based on the FEM simulations and phase transformation behavior deduced form the small samples, the disk heat treatment was chosen to be T_α − 5 °C/30 min plus T_α + 17 °C/5 min; a final heat treatment at 1100 °C was also used during the heat treatment to effect lamellar decomposition of the high-temperature alpha phase prior to air cooling to room temperature. For the supertransus heating step, it was estimated that approximately 2 of the 5 minutes comprised the initial heating transient, and that the disk was within 5 °C of the su-

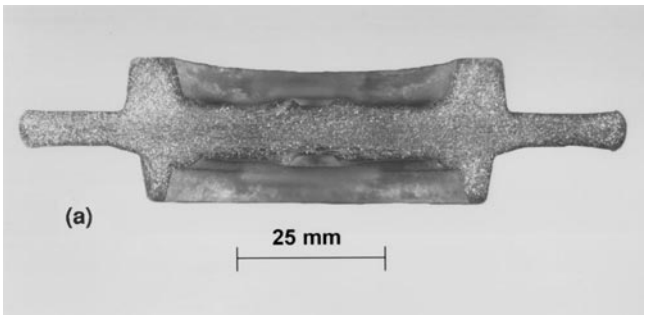

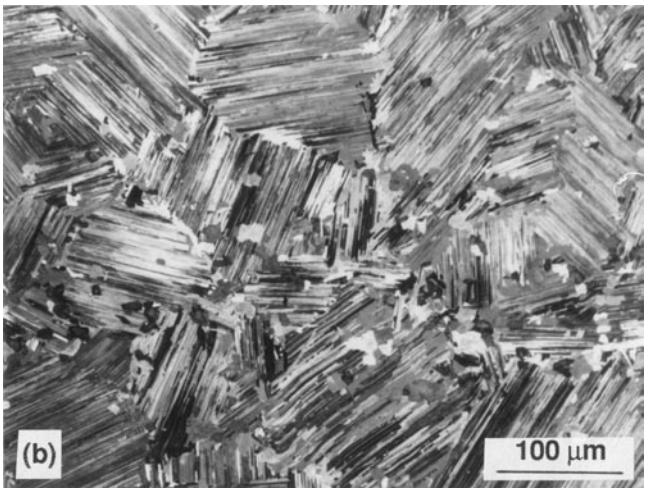

Fig. 11—Subscale disk forging of Ti-45Al-2Cr-2Nb heat treated at T_α − 5 °C (1285 °C) for 30 min followed by T_α + 17 °C (1307 °C) for 5 min and finally 1100 °C for 2 min: (*a*) macrostructure and (*b*) typical microstructure.

pertransus furnace temperature for 3 minutes. Furthermore, based on the measured gamma particle dissolution time at T_α + 17 °C of approximately 1 minute (Table II), it was estimated that noticeable alpha grain growth would occur during the final 2 minutes of the supertransus heat treatment.

The macrostructure and a typical microstructure of the heat-treated subscale disk are shown in Figure 11. The macrostructure (Figure 11(a)) showed excellent uniformity. Microstructural examination (Figure 11(b)) revealed a largely lamellar morphology with a small volume fraction of gamma. Assuming that the lamellar colony and prior-alpha grain sizes are equivalent, the measured colony size (≈125 μm) in the disk microstructure is very similar to the alpha grain size predicted from the grain growth results for T_α + 17°C at a time equal to 2 minutes following the completion of gamma particle dissolution. The small amount of single-phase gamma seen in the microstructure in Figure 11(b) is believed to have been formed during the cooling sequence *following* supertransus heat treatment.[30]

Similar results were obtained during the heat treatment of the large Ti-46.7Al-2Cr-2Nb forging. The cycle for this alloy comprised T_α − 20 °C/40 minutes followed by T_α + 30 °C/7 minutes and then air cooling; air cooling was used to avoid the development of large temperature gradients in the forging and, thus, possible cracking. Approximate heat-transfer calculations using the Heisler

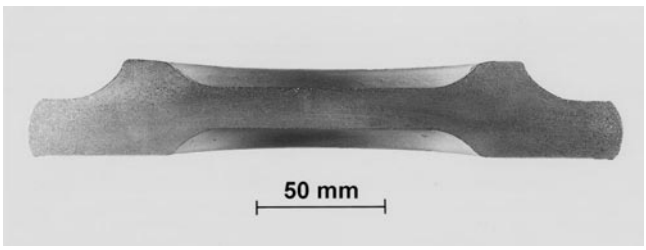

Fig. 12—Macrostructure of full-scale Ti-46.7Al-2Cr-2Nb isothermal forging heat treated at T_α − 20 °C (1320 °C) for 40 min followed by T_α + 30 °C (1370 °C) for 7 min and then air cooled.

diagrams established that surface-to-center temperature differences during the supertransus heating step would be a maximum of 6 °C (thinnest areas) to 12 °C (thickest areas), and that the lag time between the center and surface temperature *vs* time curves would be on the order of 1 minute. By referring to the grain growth curves in Figure 10, lag times of this order of magnitude could be expected to give rise to grain size *variations* from the surface to the center on the order of 30 μm for average grain sizes over 120 μm. Such grain size variations would be difficult to measure, as indeed was confirmed by observations of the macrostructure (Figure 12) and relatively uniform microstructures in the heat-treated forging.

V. SUMMARY AND CONCLUSIONS

Samples of two wrought, near-gamma titanium aluminide alloys ranging in size from laboratory coupons to full-scale forgings were given a two-step (subtransus/supertransus) heat treatment to establish the kinetics of gamma phase dissolution and alpha grain growth and the technical feasibility of process scaleup. The following conclusions were drawn from this work.

1. Subtransus heat treatment just below the alpha transus gives rise to a microstructure of equiaxed alpha grains pinned by remnant gamma particles. The limiting size of the alpha grains can be predicted by the model of Hazzledine and Oldershaw.[28]
2. Microstructure development during a supertransus heat treatment immediately following the subtransus heat-treatment results in the dissolution of remnant gamma particles, after which rapid growth of single-phase alpha grains occurs. Prior to complete dissolution of the gamma particles, relatively little alpha grain growth occurs, as predicted by the application of the results of the Hazzledine and Oldershaw model in conjunction with an assumption of uniform dissolution of all remnant gamma particles.
3. The observed kinetics of gamma particle dissolution during supertransus heat treatment are better predicted by a diffusion analysis; an interface reaction model greatly overestimates the required dissolution times.
4. The short-time kinetics of alpha grain growth follow the same trend as the longer time grain growth kinetics measured previously.
5. Within the limits determined by temperature uniformity and heating rate, full scale forgings can be supertransus heat treated to produce microstructures with small-to-moderate alpha grain sizes.

ACKNOWLEDGMENTS

This work was conducted as part of the in-house research activities of the Metals, Ceramics, and NDE Division of the Materials and Manufacturing Directorate of the Air Force Research Laboratory (formerly Wright Laboratory). The longstanding support and encouragement of the Directorate management and the Air Force Office of Scientific Research (Captain Charles Ward, program manager) are gratefully acknowledged. Work by two of the authors (VS and KHGA) was supported under Air Force Contract Nos. F33615-92-C-5900 and F33615-94-C-5804. The authors thank General Electric Aircraft Engines (J. Chesnutt and C. Austin), Wyman-Gordon/Houston (W. Konkel), and Ladish (D. Furrer), who provided the isothermal forgings used in this work. The performance and completion of this work would not have been possible without the yeoman service of P. Fagin, who performed the experimental work with the greatest of care; M. Simon, who conducted the reaction kinetics simulations; R.L. Goetz, who performed the FEM analysis of the heat treatments for the disk forgings; and L. Farmer and J. Paine, who prepared the manuscript with great patience and professionalism. The authors acknowledge their efforts with the sincerest of thanks and appreciation.

REFERENCES

1. Y.-W. Kim: *JOM*, 1994, vol. 46 (7), pp. 30-39.
2. S.L. Semiatin: in *Gamma Titanium Aluminides*, Y.-W. Kim, R. Wagner, and M. Yamaguchi, eds., TMS, Warrendale, PA, 1995, pp. 509-24.
3. S.L. Semiatin, V. Seetharaman, and V.K. Jain: *Metall. Mater. Trans. A*, 1994, vol. 25A, pp. 2753- 68.
4. K. Wurzwallner, H. Clemens, P. Schretter, A. Bartels, and C. Koeppe: in *High-Temperature Ordered Intermetallic Alloys V*, I. Baker, R. Darolia, J.D. Whittenberger, and M.H. Yoo, eds., MRS, Pittsburgh, PA, 1993, pp. 867-72.
5. P.L. Martin, C.G. Rhodes, and P.A. McQuay: in *Structural Intermetallics*, R. Darolia, J.J. Lewandowski, C.T. Liu, P.L. Martin, D.B. Miracle, and M.V. Nathal, eds., TMS, Warrendale, PA, 1993, pp. 177-86.
6. S.L. Semiatin and V. Seetharaman: *Metall. Mater. Trans. A*, 1995, vol. 26A, pp. 371-82.
7. R.M. Imayev, O.A. Kaibyshev, and G.A. Salishev: *Acta Metall. Mater.*, 1992, vol. 40, pp. 581-87.
8. C.M. Lombard, A.K. Ghosh, and S.L. Semiatin: in *Gamma Titanium Aluminides*, Y.-W. Kim, R. Wagner, and M. Yamaguchi, eds., TMS, Warrendale, PA, 1995, pp. 579-86.
9. Y.-W. Kim: *Mater. Sci. Eng.*, 1995, vols. A192–A193, pp. 519-33.
10. Y.-W. Kim and D.M. Dimiduk: U.S. Patent 5,226,985, July 13, 1993.
11. Y.-W. Kim: Wright Laboratory Materials Directorate, Wright-Patterson Air Force Base, OH, unpublished research, 1996.
12. C.T. Liu, J.H. Schneibel, P.J. Maziasz, J.L. Wright, and D.S. Easton: *Intermetallics*, 1996, vol. 4, pp. 429-40.
13. J.P. Holman: *Heat Transfer*, McGraw-Hill Book Company, New York, NY, 1986, ch. 4.
14. M.P. Heisler: *Trans. ASME*, 1947, vol. 69, pp. 227-36.
15. J.B. Henderson and H. Groot: Technical Report No. TPRL 1284, Thermophysical Properties Research Laboratory, Purdue University, West Lafayette, IN, 1993.
16. S.L. Semiatin, R. Nekkanti, M.K. Alam, and P.A. McQuay: *Metall. Trans. A*, 1993, vol. 24A, pp. 1295-1306.
17. H.B. Aaron and G.R. Kotler: *Metall. Trans.*, 1971, vol. 2, pp. 393-408.
18. S.L. Semiatin and P.A. McQuay: *Metall. Trans. A*, 1992, vol. 23A, pp. 149-61.
19. W. Sprengel, H. Nakajima, and H. Oikawa: *Mater. Sci. Eng.*, 1996, vol. A213, pp. 45-50.
20. M.J. Whelan: *Met. Sci. J.*, 1969, vol. 3, pp. 95-97.
21. G. Grewal and S. Ankem: *Metall. Trans. A*, 1989, vol. 20A, pp. 39-54.
22. G. Grewal and S. Ankem: *Metall. Trans. A*, 1990, vol. 21A, pp. 1645-54.
23. G. Grewal and S. Ankem: *Acta Metall.*, 1990, vol. 38, pp. 1607-17.
24. I. Anderson and O. Grong: *Acta Metall. Mater.*, 1995, vol. 43, pp. 2673-88.
25. V. Seetharaman and S.L. Semiatin: *Metall. Mater. Trans. A*, 1997, vol. 28A, pp. 947-54.
26. C.S. Smith: *Trans. Am. Inst. Min. Eng.*, 1948, vol. 175, p. 15.
27. P. Hellman and M. Hillert: *Scand. J. Metall.*, 1975, vol. 4, p. 211.
28. P.M. Hazzledine and R.D.J. Oldershaw: *Phil. Mag. A*, 1990, vol. 61, pp. 579-89.
29. P. Wang, G.B. Viswanathan, and V.K. Vasudevan: *Metall. Trans. A*, 1992, vol. 23A, pp. 690-97.
30. V. Seetharaman and S.L. Semiatin: *Metall. Mater. Trans. A*, 1996, vol. 27A, pp. 1987-2004.